Chemical Science

ROYAL SOCIETY OF CHEMISTRY

EDGE ARTICLE

View Article Online
View Journal | View Issue

Cite this: *Chem. Sci.*, 2023, **14**, 550

All publication charges for this article have been paid for by the Royal Society of Chemistry

Received 24th August 2022
Accepted 14th December 2022

DOI: 10.1039/d2sc04729b

rsc.li/chemical-science

Multiple C–C bond formation upon electrocatalytic reduction of CO_2 by an iron-based molecular macrocycle†

Si-Thanh Dong, Chen Xu and Benedikt Lassalle-Kaiser *

Molecular macrocycles are very promising electrocatalysts for the reduction of carbon dioxide into value-added chemicals. Up to now, most of these catalysts produced only C_1 products. We report here that iron phthalocyanine, a commercially available molecule based on earth-abundant elements, can produce light hydrocarbons upon electrocatalytic reduction of CO_2 in aqueous conditions and neutral pH. Under applied electrochemical potential, C_1 to C_4 saturated and unsaturated products are evolved. Isotopic labelling experiments unambiguously show that these products stem from CO_2. Control experiments and *in situ* X-ray spectroscopic analysis show that the molecular catalyst remains intact during catalysis and is responsible for the reaction. On the basis of experiments with alternate substrates, a mechanism is proposed for the C–C bond formation step.

Introduction

Atmospheric carbon dioxide (CO_2) has been used as a feedstock to produce all biomass,[1] including fossil fuels, since photosynthesis developed on Earth more than two billion years ago. Industrialized societies are eagerly searching for such a solar-to-chemical conversion process, which would help mitigate their carbon dioxide emissions while providing alternative ways to produce staple chemicals.[2] The electrochemical CO_2 reduction reaction (CO_2RR) has been proposed as a viable technology to convert this gas into valuable chemicals. At present, the most common products of CO_2 reduction are carbon monoxide (CO) and formic acid (HCOOH). Although these C_1 products are near the market-ready level, they only reflect a few of the chemicals that can be generated from CO_2.[3] Great efforts have been directed to further reduce CO_2 to higher value products, particularly those including C–C bonds. Starting from the work of Hori and co-workers[4] in the 80s, copper-based catalysts have shown remarkable activity towards the formation of light hydrocarbons, such as methane and ethylene.[5] Despite these performances, the precise nature of the active sites involved remains debatable,[6] partly because of the restructuring of copper during catalysis.[7,8] Recently, single-atom catalysts (SACs) have gained significant attention in the field of CO_2 reduction due to their low metal content and high activity.[9] While the reduction of CO_2 on SACs yields mostly CO, other more reduced products have been obtained,[10,11] including C_{2+} products such as ethanol[12] and acetone.[13] Although SACs properties are expected to be favorable to the reduction of CO_2 beyond CO,[14] the heterogeneity of their structures[9] prevents establishing detailed reaction mechanisms.

Molecular complexes catalyze the reduction of CO_2 to CO with high efficiency and stability,[15,16] and the homogeneity of their chemical structure allows establishing precise reaction mechanisms.[17,18] Transition metal macrocycles such as porphyrins[19] or phthalocyanines[20–23] have shown very promising results in the electrochemical reduction of CO_2, both as homogeneous[23] and heterogeneous systems.[24] Beside their efficiency and robustness, these molecular catalysts also offer chemical tunability, which allows orienting their reactivity towards higher turnover numbers (TONs),[25] higher selectivity,[26] or the synthesis of a specific compound.[27] While most molecular species catalyzed the CO_2 to CO reduction, a handful of examples have shown that C_1 products such as methane[28,29] or methanol[21,30] can be produced by catalysts with M–N_4 structure. Ethanol and acetic acid were found as a product of CO_2 reduction on cobalt and manganese corrole species, respectively.[31,32] There is, however, no example of C_{2+} compounds produced from CO_2 reduction by a catalyst for which the molecular nature during catalysis is demonstrated.

We report here on the electrocatalytic formation of saturated and unsaturated light hydrocarbons (C_1–C_4) from CO_2 using a heterogenized molecular iron phthalocyanine catalyst in a flowing system (see Fig. 1 and S1†). The analysis of the products formed under applied electrochemical potential shows that, besides CO and H_2, small amounts of methane, ethylene, ethane, propene, propane, and *n*-butane are detected along with traces of C_5 products. Electrocatalytic experiments using alternate substrates such as carbon monoxide (CO) or

Synchrotron SOLEIL, Route Départementale 128, l'Orme des Merisiers, 91190 Saint-Aubin, France. E-mail: benedikt.lassalle@synchrotron-soleil.fr

† Electronic supplementary information (ESI) available. See DOI: https://doi.org/10.1039/d2sc04729b

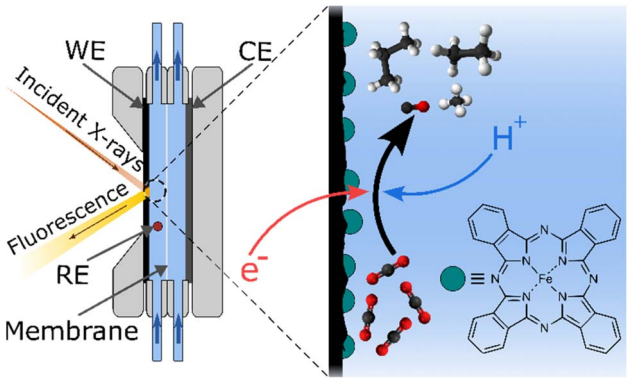

Fig. 1 Schematic side view of the electrochemical cell and simplified CO_2 reduction process on the surface of the working electrode. The dark green circles represent iron phthalocyanine (FePc), the molecular catalyst used in this study, whose structure is shown in the right corner. WE, CE, and RE stand for "working electrode", "counter electrode", and "reference electrode", respectively. The scheme is not drawn to scale.

formaldehyde (HCHO) support a mechanism involving a terminal carbene as a critical species on the way to C_{2+} compounds.

Results and discussion

Electrocatalysis and distribution of products

Based on the design of Ager and co-workers,[33] CO_2 reduction experiments were performed in an electrocatalytic flow cell consisting of two chambers for the cathodic and anodic reactions, separated by a Nafion® membrane (see Fig. 1 and S1†). The cathode consists of a glassy carbon electrode, on which an ink containing iron phthalocyanine (FePc) and a carbon powder is drop-casted with a surface concentration of around 80 nmol cm^{-2} (see ESI† for electrode preparation procedure). A reference electrode is arranged in the cathode chamber, and the anode consists of a nickel plate. Two independent reservoirs contain the catholyte and anolyte ($KHCO_3$ 0.1 M), which are flown independently in the anodic and cathodic chambers. The headspace of the cathodic compartment is analyzed during the experiment by an online gas chromatograph that performs automatic sampling every thirty minutes (see Fig. S2A†).

Fig. 2A shows the chronoamperometric curves of constant potential electrolysis under Ar or CO_2 for two hours. After poising an FePc-modified electrode at −1.1 V *vs.* RHE under a CO_2 atmosphere, peaks corresponding to ethylene (C_2H_4), ethane (C_2H_6), propene (C_3H_6), propane (C_3H_8) and *n*-butane (C_4H_{10}) clearly stand out in the chromatogram (see Fig. 2B). Other peaks corresponding to unsaturated C_4 as well as *n*-pentane and unsaturated C_5 products can also be observed, although with a lower intensity. Methane (CH_4) is also clearly present on another module of the gas chromatograph (see Fig. S3†). The catholyte was analyzed by ^1H NMR to check for liquid products, but none was detected (see Fig. S4†). Control experiments were performed to ensure that FePc catalyzed the reduction of CO_2 into the products observed. When a FePc-modified electrode was set under catalytic conditions in an

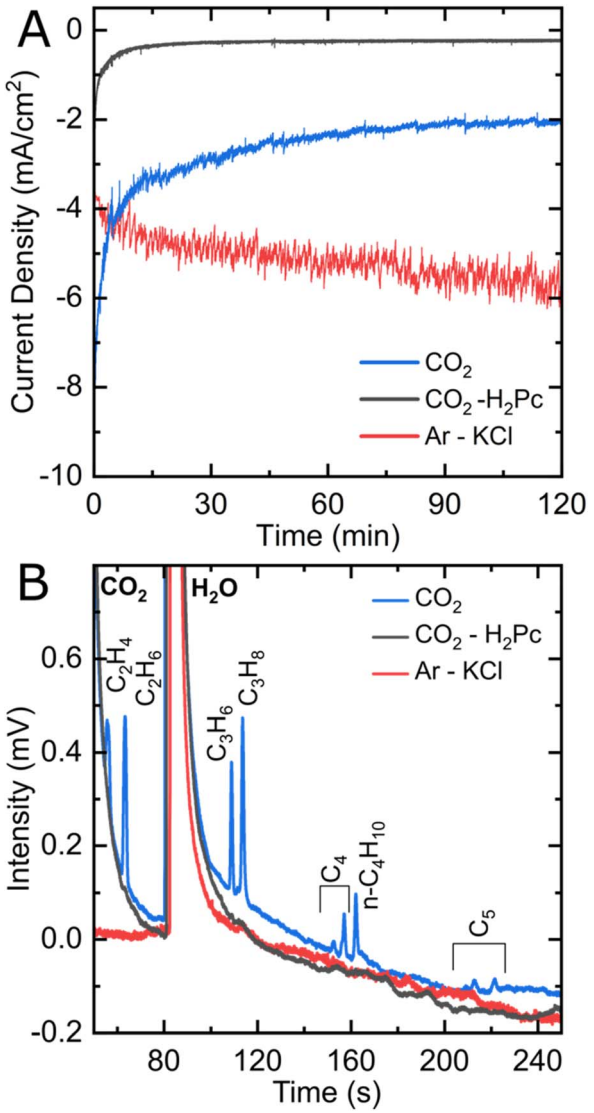

Fig. 2 (A) Chronoamperometric curves and (B) module B gas chromatograms of FePc-modified electrodes under Ar in 0.1 M KCl (red) and CO_2 in 0.1 M $KHCO_3$ (blue) and an H_2Pc-modified electrode under CO_2 in $KHCO_3$ (black). Chronoamperometric experiments are performed at −1.1 V *vs.* RHE for two hours, after which a gas chromatograph (GC) samples their resulting gaseous products.

Ar-saturated $KHCO_3$ electrolyte, hydrogen was the major product detected after two hours of electrolysis, with a trace amount of CO and hydrocarbons (see Fig. S5†). The observed carbon products can be attributed to the small amount of CO_2 that exists in equilibrium with the $KHCO_3$ electrolyte. In fact, a similar FePc-modified electrode, at the same potential, under a CO_2-free environment (Ar-saturated 0.1 M KCl electrolyte), produces only H_2 (see Fig. 2B and S3†). The current density observed is higher than under CO_2 (see Fig. 2A), indicating a high activity of FePc towards hydrogen evolution in a CO_2-free environment at high overpotential. When an H_2Pc-modified electrode was poised at −1.1 V in a CO_2-saturated $KHCO_3$ electrolyte, a twenty-fold decrease in current density was observed as compared to an FePc-modified electrode, indicating

a negligible catalytic activity without the Fe center. In agreement with the low catalytic activity, the main product detected was H_2, with a miniscule amount of CO (Fig. S3†). These results strongly indicate CO_2 as the source of the carbon products observed and underline the essential role of the metal center in the catalytic process.

To confirm the origin of the carbon atoms in the C_{2+} products observed in the chromatograms, gas chromatography coupled mass spectrometry (GC-MS) experiments were performed. Fig. 3 shows the GC-MS chromatograms corresponding to the retention time of C_4 products (190–240 s). We focus on the C_4H_8 signal since it has the highest intensity of all C_4 products without overlapping the signal of CO_2 or CO. The $m/z = 56$ mass, which corresponds to a C_4H_8 species containing four ^{12}C atoms, shows a peak when $^{12}CO_2$ is used as the substrate, while it does not appear in the presence of $^{13}CO_2$. The opposite behavior is observed with the $m/z = 60$ mass, which corresponds to a C_4H_8 species with four ^{13}C atoms. The GC-MS chromatogram of the $m/z = 41$ mass at the region of the retention time of C_3 and C_4 products is shown on Fig. S6.† The $m/z = 41$ mass, which corresponds to a C_3H_5 fragment (originating from both C_3 and C_4 products) shows two distinguishable peaks when $^{12}CO_2$ is used, which disappear with $^{13}CO_2$. These isotopic labelling experiments demonstrate that the origin of the carbon atoms in the hydrocarbons observed is indeed CO_2.

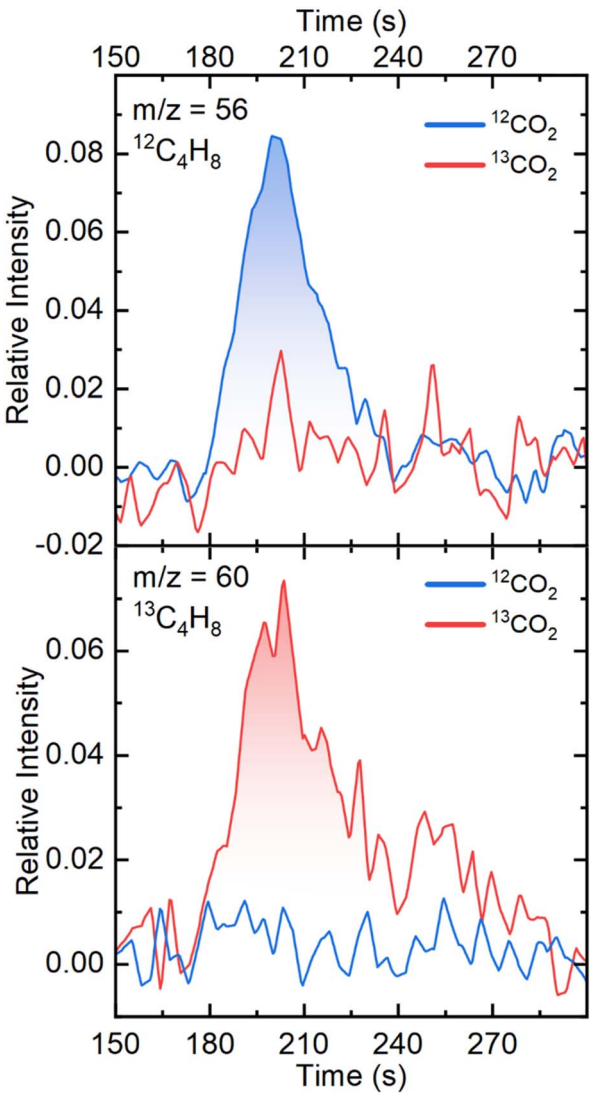

Fig. 3 GC-MS chromatograms for mass $m/z = 56$ of $^{12}C_4H_8$ and mass $m/z = 60$ of $^{13}C_4H_8$ at the retention time of C_4 products. Chronoamperometric experiments were performed on FePc-modified electrodes at −1.1 V *vs.* RHE for two hours, after which the GC-MS sampled the resulting gaseous products. The chromatograms were averaged from three independent experiments.

Fig. 4 shows the product distribution in terms of faradaic efficiency (FE) for each of the products obtained after a 2 hours electrocatalytic experiment under CO_2. The potential range is chosen where there is significant CO_2 reduction activity without generating hydrogen bubbles that would make the system unstable. Between −0.7 V and −0.9 V, CO and H_2 are the only products observed. Although the current density at high overpotential slightly decreases over time, the selectivity of all products remains constant (see Fig. S7†). The amount of hydrogen increases steadily from −0.7 V to −1.1 V up to 65% FE at the expense of CO. Noticeable amounts of hydrocarbons can be observed starting from −0.9 V, methane being the main of them with up to 4% at −1.0 and −1.1 V. Ethylene, ethane, propene, propane and *n*-butane are produced with faradaic efficiencies of 0.1–0.25% each, making the total of C_{2+} products to be around 1%. It should be noted that the amount of ethylene is underestimated because of the high background generated by CO_2 in the chromatograph column. Despite the low amounts of products generated, their distribution was reproducible, as shown by the replicates performed on three different electrodes.

Catalyst characterization

In order to determine the nature of the catalyst under operating conditions and check its integrity, we performed *in situ* and *operando* X-ray absorption spectroscopy (XAS) experiments at the iron K-edge in the exact same electrochemical cell (see Fig. 1, S1 and S2B†). Fig. 5 shows the X-ray absorption near-edge structure (XANES) spectra of the FePc-modified electrode under open circuit potential (OCP) and under catalytic conditions, in a CO_2 atmosphere, with the corresponding non-normalized spectra in Fig. S8.† The spectrum of the electrode under resting state presents the same features as the pure, starting compound, showing the chemical robustness of the FePc catalyst after dropcasting and in the presence of an electrolyte. When poising the electrode at a potential of −1.1 V (at which C_{2+} products are observed), the spectrum shows a shift to lower energies (−2.7 eV at half-edge jump) while keeping the features that are characteristic of phthalocyanines,[34] *i.e.* two pre-edge peaks at 7114 eV and 7118 eV. A XANES spectrum was also recorded *in situ* after performing electrocatalytic experiments under a CO_2 atmosphere, and it was remarkably similar to the one collected on the starting electrode. The non-normalized spectra indicate a 10% material loss after 4.5 hours of continuous flowing, which is standard in this type of experiment.[35] The comparison between the spectra collected under *in situ* and

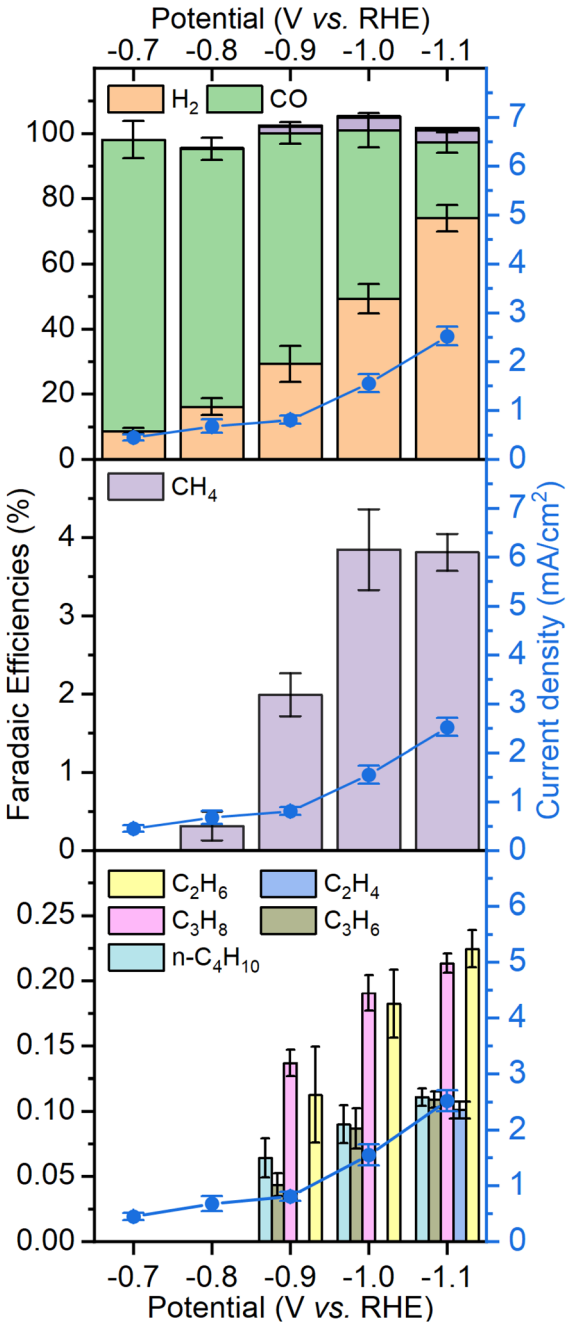

Fig. 4 Product distribution observed as faradaic efficiencies with FePc-modified electrodes as a function of applied potential. The total current density is plotted for each potential as the blue lines. The amount of ethylene (C_2H_4) is underestimated due to the high background generated by CO_2 in the chromatograph column.

operando conditions and those of reference compounds (metallic iron, Fe_3O_4) clearly rule out the presence of metallic iron or iron oxide nanoparticles that would be produced by the decomposition of the molecular catalyst. Altogether, these spectroscopic data collected under *in situ* conditions clearly demonstrate the molecular nature and the stability of the catalyst throughout the experiment.

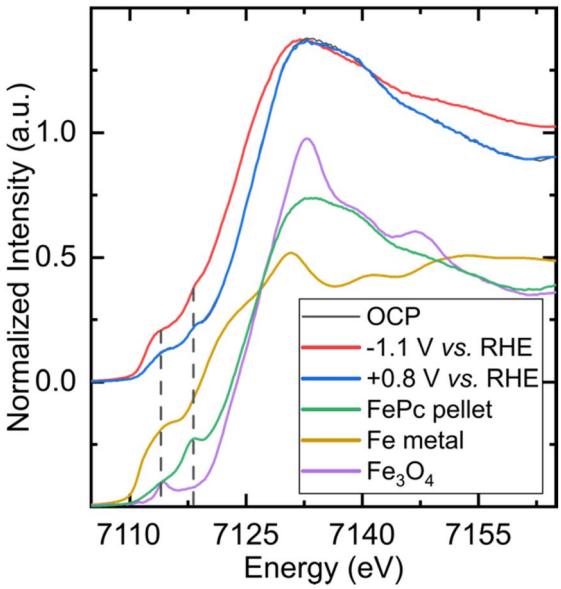

Fig. 5 *In situ* and *operando* X-ray absorption spectra collected on an FePc-modified electrode under different conditions and on reference samples. The spectra at the top correspond to an FePc-modified electrode under a CO_2 atmosphere poised at of FePc (green), on a metallic sheet of iron (gold), and on a pellet of Fe_3O_4 (purple). The two dashed lines indicate the pre-edge features of FePc at 7114 eV and 7118 eV. OCP (black), at −1.1 V *vs.* RHE (red) and going back at +0.8 V *vs.* RHE (blue). The spectra at the bottom correspond to *ex situ* reference spectra collected on a pellet.

In addition, infrared (IR) spectra were recorded on the FePc catalyst powder and FePc-modified electrodes before and after electrolysis at −1.1 V *vs.* RHE (see Fig. S9†). The spectra recorded show close similarity, agreeing with the XAS results concerning the stability of the catalyst during electrolysis.

C–C bond formation mechanism

The demonstration that a molecular electrocatalyst can form several consecutive C–C bonds poses the question of their formation mechanism. Since the major product observed upon reduction of CO_2 is CO, we postulated that the first intermediate for the formation of C–C bonds could be an FePc–CO species (see Fig. 6). Indeed, electrolysis with CO as substrate shows the formation of similar hydrocarbon products as observed for CO_2, albeit with faradaic efficiencies approximately twice as low (see Fig. S10†). We attribute this lower faradaic efficiency to the low solubility of CO in water (1 mM) as compared to that of CO_2 (33 mM). As observed in other studies,[33,36] we surmised that the difference in initial concentration of substrate was responsible for this difference in efficiency and performed finite element calculations to simulate concentration profiles upon CO_2 reduction. The results show that the concentration of CO generated by CO_2 reduction within 5 μm from the working electrode ranges from 1.5 to 4.5 mM (see ESI†), supporting a relationship between the amount of C_{2+} products and the local concentration of CO. These experiments confirm that FePc–CO is indeed an intermediate on the way to C_{2+} products.

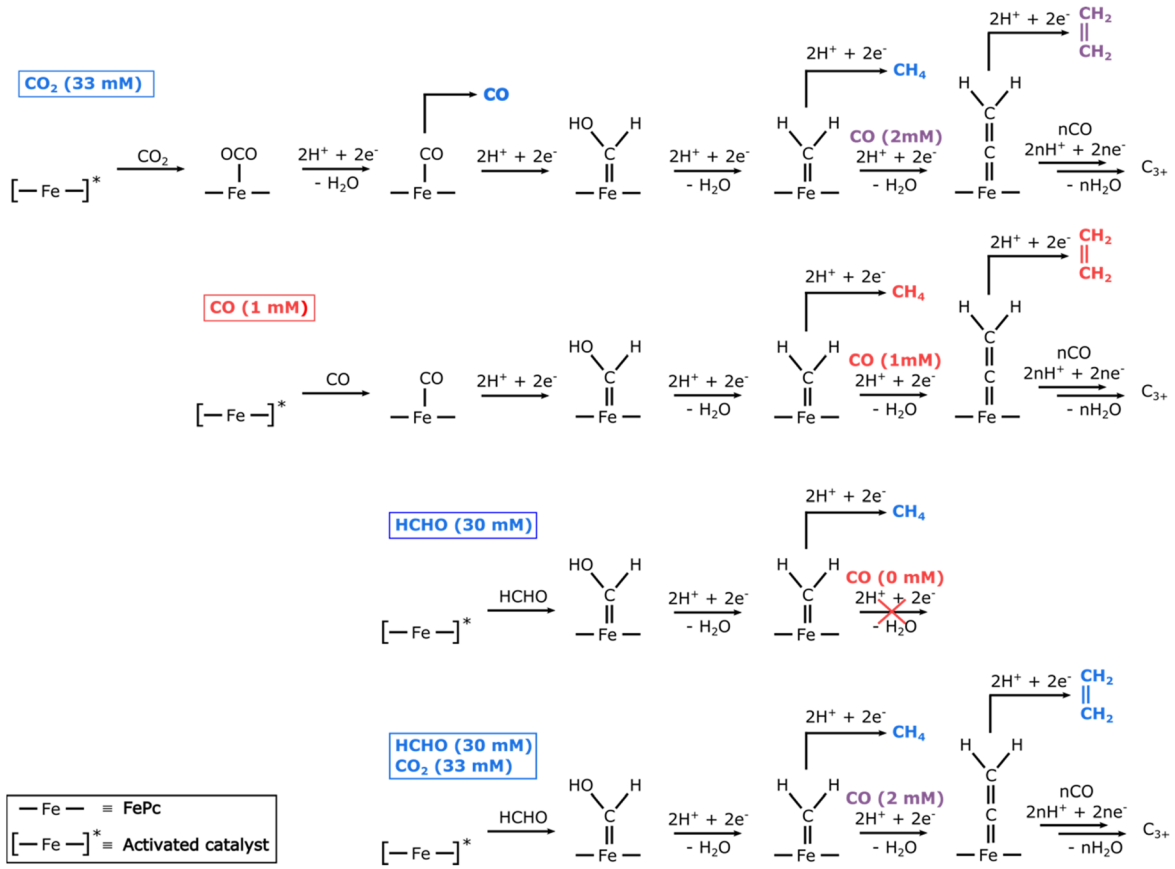

Fig. 6 Simplified mechanisms proposed for the formation of C–C bonds by FePc with either CO_2, CO, HCHO, or a mixture of HCHO and CO_2 as substrates. The colour code for substrates and products is as follow: blue, purple, and red for high, intermediate, and low concentrations, respectively.

By analogy with what happens during the Fischer–Tropsch synthesis of long-chain hydrocarbons, we hypothesized that a terminal FePc=CH_2 carbene species could be the precursor to all C_{2+} products. This transient species would be formed, *via* a hydroxycarbene species, by reaction of an FePc–CO adduct with either H_2 formed locally or with protons and electrons available in large amounts. This species would then further react either with more H_2 (or protons and electrons) to form methane. To form a C–C bond, the iron carbene species undergo CO insertion similar to Fischer–Tropsch mechanism. This CO insertion pathway is different from the carbene coupling involved in the formation of ethylene on metallic copper since there are no adjacent active sites in iron phthalocyanine. The process could continue a few times following various pathways and lead to the formation of longer saturated or unsaturated hydrocarbon chains (see Fig. 6).

To verify this hypothesis, we used formaldehyde as a substrate, expecting it to form an FePc=CH(OH) hydroxycarbene species by direct reaction with the activated form of the catalyst[37] (see Fig. 6). In these conditions, the product distribution shows similar multi-carbon products as with CO_2 or CO as substrates, although in much lower amounts (Fig. S10†), as well as methane (2%) and traces of methanol (Fig. S10 and S13†). While the concentration of formaldehyde (30 mM) is similar to that of saturated CO_2 in water at 25 °C (33 mM), the very low faradaic efficiencies observed for C_{2+} products can be explained by the absence of any CO to be inserted in the FePc=C bond of the putative carbene species. Without any CO to react further, the carbene species is preferentially reduced into methane, leading to a 6-fold increase in the faradaic yield of methane as compared to the CO substrate. In order to confirm the reaction of CO with an FePc carbene species, we performed electrolysis with HCHO in a CO_2 atmosphere, as CO_2 reduction could provide the necessary CO to increase the C_{2+} formation with the carbene species generated from HCHO. Indeed, at −1.1 V *vs.* RHE, the total faradaic efficiency of C_{2+} products is one order of magnitude higher than observed in HCHO without CO_2 (see Fig. S11 and S12†), thus confirming our hypothesis of a reaction between CO and a carbene species obtained from formaldehyde. At less negative potentials, where the formation of CO from CO_2 is more favorable, the total C_{2+} faradaic efficiency increases further, reaching a maximum value of 1.5% at −0.9 V *vs.* RHE, *ca.* three times higher than when only CO_2 is used as substrate (see Fig. S12†). The higher selectivity of C_{2+} products after electrolysis of HCHO under CO_2 clearly supports the hypothesis that the formation of C_{2+} species

involves CO insertion on an intermediate FePc carbene species, as described in Fig. 6.

The existence of an FePc=CH_2 intermediate on the way to C_{2+} products is supported by the fact that several carbene species of iron porphyrin (a macrocycle similar to FePc) have been reported, either as transient[38,39] or stable species,[40] and that FePc itself has been reported as an efficient catalyst for the cyclopropanation of alkenes,[41] which involves FePc–carbene intermediates. Iron porphyrins are also known for catalyzing the insertion of carbenes into N–H, S–H, or C–H bonds.[42,43] These precedents, as well as the experiments described here with alternate substrates, strongly support the involvement of an FePc carbene species on the way to C_{2+} hydrocarbons.

Conclusions

We reported in this paper on the electrocatalytic activity of iron phthalocyanine, a molecular macrocycle based on earth-abundant elements, towards the reduction of CO_2 into light hydrocarbons with up to three C–C bonds. Using *operando* X-ray absorption spectroscopy, we showed that the catalyst keeps its molecular structure throughout the electrocatalytic process. Based on experiments involving carbon monoxide or formaldehyde, we showed that the local concentration of CO is key to the formation of C–C bonds and propose a terminal carbene as an intermediate on the way to C_{2+} products. These results indicate that the formation of several consecutive carbon–carbon bonds can be catalyzed by single-site transition metal macrocycles under mild electrochemical conditions. The mechanistic insights that we provided open a perspective for the design of both molecular and material-based catalysts with enhanced selectivity towards C_2+ products.

Data availability

The authors confirm that the data supporting the findings of this study are available within the article and its ESI material.† Raw data that support the findings of this study are available from the corresponding author, upon reasonable request.

Author contributions

Conceptualization: STD, BLK investigation: STD, CX funding acquisition: BLK supervision: BLK writing – original draft: STD, BLK writing – review & editing: STD, BLK.

Conflicts of interest

There are no conflicts to declare.

Acknowledgements

We express our gratitude to Dr Jean-Blaise Brubach of the AILES beamline of Synchrotron SOLEIL for his help during infrared spectra collection. We are indebted to Ms. Chanjuan Zhang and Dr Zakaria Halime at the Institut de Chimie Moléculaire et des Matériaux d'Orsay, Université Paris-Saclay for their assistance in performing ^{1}H-NMR measurements. The Agence Nationale de la recherche is acknowledged for a young researcher grant to B. L.-K. (grant no. 18-CE05-0007).

References

1 A. A. Benson, J. A. Bassham, M. Calvin, T. C. Goodale, V. A. Haas and W. Stepka, *J. Am. Chem. Soc.*, 1950, **72**, 1710–1718.
2 J. Cheon, J. Y. Yang, M. Koper and O. Ishitani, *Acc. Chem. Res.*, 2022, **55**, 931–932.
3 O. S. Bushuyev, P. De Luna, C. T. Dinh, L. Tao, G. Saur, J. van de lagemaat, S. O. Kelley and E. H. Sargent, *Joule*, 2018, **2**, 825–832.
4 Y. Hori, K. Kikuchi, A. Murata and S. Suzuki, *Chem. Lett.*, 1986, **15**, 897–898.
5 S. Nitopi, E. Bertheussen, S. B. Scott, X. Liu, A. K. Engstfeld, S. Horch, B. Seger, I. E. L. Stephens, K. Chan, C. Hahn, J. K. Nørskov, T. F. Jaramillo and I. Chorkendorff, *Chem. Rev.*, 2019, **119**, 7610–7672.
6 D. Raciti and C. Wang, *ACS Energy Lett.*, 2018, **3**, 1545–1556.
7 J. Vavra, T.-H. Shen, D. Stoian, V. Tileli and R. Buonsanti, *Angew. Chem.*, 2021, **133**, 1367–1374.
8 Y.-G. Kim, J. H. Baricuatro and M. P. Soriaga, *Electrocatalysis*, 2018, **9**, 526–530.
9 J. Zhang, W. Cai, F. Xin Hu, H. Yang and B. Liu, *Chem. Sci.*, 2021, **12**, 6800–6819.
10 L. Han, S. Song, M. Liu, S. Yao, Z. Liang, H. Cheng, Z. Ren, W. Liu, R. Lin, G. Qi, X. Liu, Q. Wu, J. Luo and H. L. Xin, *J. Am. Chem. Soc.*, 2020, **142**, 12563–12567.
11 W. Ju, A. Bagger, X. Wang, Y. Tsai, F. Luo, T. Möller, H. Wang, J. Rossmeisl, A. S. Varela and P. Strasser, *ACS Energy Lett.*, 2019, **4**, 1663–1671.
12 Y. Jiao, Y. Zheng, P. Chen, M. Jaroniec and S.-Z. Qiao, *J. Am. Chem. Soc.*, 2017, **139**, 18093–18100.
13 K. Zhao, X. Nie, H. Wang, S. Chen, X. Quan, H. Yu, W. Choi, G. Zhang, B. Kim and J. G. Chen, *Nat. Commun.*, 2020, **11**, 2455.
14 A. Bagger, W. Ju, A. S. Varela, P. Strasser and J. Rossmeisl, *Catal. Today*, 2017, **288**, 74–78.
15 S. Ren, D. Joulié, D. Salvatore, K. Torbensen, M. Wang, M. Robert and C. P. Berlinguette, *Science*, 2019, **365**, 367–369.
16 X. Zhang, Y. Wang, M. Gu, M. Wang, Z. Zhang, W. Pan, Z. Jiang, H. Zheng, M. Lucero, H. Wang, G. E. Sterbinsky, Q. Ma, Y.-G. Wang, Z. Feng, J. Li, H. Dai and Y. Liang, *Nat. Energy*, 2020, **5**, 684–692.
17 J. Bonin, A. Maurin and M. Robert, *Coord. Chem. Rev.*, 2017, **334**, 184–198.
18 Y. Kuramochi, O. Ishitani and H. Ishida, *Coord. Chem. Rev.*, 2018, **373**, 333–356.
19 G. F. Manbeck and E. Fujita, *J. Porphyrins Phthalocyanines*, 2015, **19**, 45–64.
20 K. Kusuda, R. Ishihara and H. Yamaguchi, *Electrochim. Acta*, 1986, **31**, 657–663.

21 E. Boutin, M. Wang, J. C. Lin, M. Mesnage, D. Mendoza, B. Lassalle-Kaiser, C. Hahn, T. F. Jaramillo and M. Robert, *Angew. Chem., Int. Ed.*, 2019, **58**, 16172–16176.
22 Z. Jiang, Y. Wang, X. Zhang, H. Zheng, X. Wang and Y. Liang, *Nano Res.*, 2019, **12**, 2330–2334.
23 R. Francke, B. Schille and M. Roemelt, *Chem. Rev.*, 2018, **118**, 4631–4701.
24 N. Corbin, J. Zeng, K. Williams and K. Manthiram, *Nano Res.*, 2019, **12**, 2093–2125.
25 C. Costentin, S. Drouet, M. Robert and J.-M. Savéant, *Science*, 2012, **338**, 90–94.
26 W. W. Kramer and C. C. L. McCrory, *Chem. Sci.*, 2016, **7**, 2506–2515.
27 P. Gotico, Z. Halime and A. Aukauloo, *Dalton Trans.*, 2020, **49**, 2381–2396.
28 B. Li, L. Sun, J. Bian, N. Sun, J. Sun, L. Chen, Z. Li and L. Jing, *Appl. Catal., B*, 2020, **270**, 118849.
29 J. Shen, R. Kortlever, R. Kas, Y. Y. Birdja, O. Diaz-Morales, Y. Kwon, I. Ledezma-Yanez, K. J. P. Schouten, G. Mul and M. T. M. Koper, *Nat. Commun.*, 2015, **6**, 8177.
30 Y. Wu, Z. Jiang, X. Lu, Y. Liang and H. Wang, *Nature*, 2019, **575**, 639–642.
31 S. Gonglach, S. Paul, M. Haas, F. Pillwein, S. S. Sreejith, S. Barman, R. De, S. Müllegger, P. Gerschel, U.-P. Apfel, H. Coskun, A. Aljabour, P. Stadler, W. Schöfberger and S. Roy, *Nat. Commun.*, 2019, **10**, 3864.
32 R. De, S. Gonglach, S. Paul, M. Haas, S. S. Sreejith, P. Gerschel, U.-P. Apfel, T. H. Vuong, J. Rabeah, S. Roy and W. Schöfberger, *Angew. Chem., Int. Ed.*, 2020, **59**, 10527–10534.
33 Gurudayal, D. Perone, S. Malani, Y. Lum, S. Haussener and J. W. Ager, *ACS Appl. Energy Mater.*, 2019, **2**, 4551–4559.
34 Y. Liu, A. Deb, K. Yee Leung, W. Nie, W. S. Dean, J. E. Penner-Hahn and C. C. L. McCrory, *Dalton Trans.*, 2020, **49**, 16329–16339.
35 T. Zhao, Y. Wang, S. Karuturi, K. Catchpole, Q. Zhang and C. Zhao, *Carbon Energy*, 2020, **2**, 582–613.
36 S. Louisia, D. Kim, Y. Li, M. Gao, S. Yu, I. Roh and P. Yang, *Proc. Natl. Acad. Sci. U. S. A.*, 2022, **119**, e2201922119.
37 H. Mahmoudi, M. Mahmoudi, O. Doustdar, H. Jahangiri, A. Tsolakis, S. Gu and M. LechWyszynski, *Biofuels Engineering*, 2017, vol. 2, pp. 11–31.
38 D. Lexa, J.-M. Savéant, J.-P. Battioni, M. Lange and D. Mansuy, *Angew. Chem., Int. Ed. Engl.*, 1981, **20**, 578–579.
39 I. Artaud, N. Gregoire, P. Leduc and D. Mansuy, *J. Am. Chem. Soc.*, 1990, **112**, 6899–6905.
40 Y. Liu, W. Xu, J. Zhang, W. Fuller, C. E. Schulz and J. Li, *J. Am. Chem. Soc.*, 2017, **139**(14), 5023–5026.
41 H.-H. Liu, Y. Wang, Y.-J. Shu, X.-G. Zhou, J. Wu and S.-Y. Yan, *J. Mol. Catal. A: Chem.*, 2006, **246**, 49–52.
42 R. D. Lewis, M. Garcia-Borràs, M. J. Chalkley, A. R. Buller, K. N. Houk, S. B. J. Kan and F. H. Arnold, *Proc. Natl. Acad. Sci. U. S. A.*, 2018, **115**, 7308–7313.
43 C. Empel, S. Jana and R. M. Koenigs, *Molecules*, 2020, **25**, 880.